Phys. Status Solidi B **246**, No. 11–12, 2553–2557 (2009) / **DOI** 10.1002/pssb.200982312

physica status solidi b
www.pss-b.com
basic solid state physics

Graphene quantum dots in perpendicular magnetic fields

J. Güttinger*[,1], C. Stampfer[1,2], T. Frey[1], T. Ihn[1], and K. Ensslin[1]

[1] Solid State Physics Laboratory, ETH Zurich, 8093 Zurich, Switzerland
[2] JARA-FIT and II. Institute of Physics, RWTH Aachen, 52074 Aachen, Germany

Received 30 April 2009, accepted 24 September 2009
Published online 12 November 2009

PACS 72.80.Rj, 73.21.La, 73.22.–f, 75.75.−c

* Corresponding author: e-mail guettinj@phys.ethz.ch, Phone: +41 44 6332836, Fax: +41 44 6331146

We report transport experiments on graphene quantum dots (QDs). We focus on excited state spectra in the near vicinity of the charge neutrality point and signatures of the electron–hole crossover as a function of a perpendicular magnetic field. Coulomb blockade resonances of a 50 nm wide and 80 nm long dot are visible at all gate voltages across the transport gap ranging from hole to electron transport. The magnetic field dependence of more than 40 states as a function of the back gate voltage can be interpreted in terms of the unique evolution of the diamagnetic spectrum of a graphene dot including the formation of the $E = 0$ Landau level, situated in the centre of the transport gap, and marking the electron–hole crossover. Around the crossover, excited states and cotunneling features are studied for varying perpendicular magnetic field.

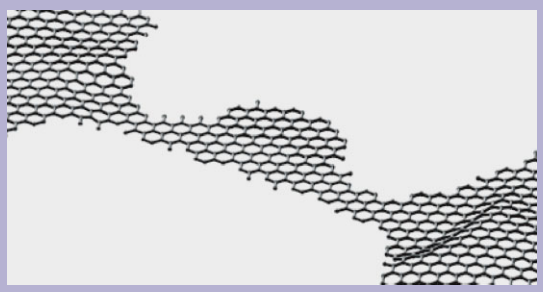

Schematic illustration of an etched graphene quantum dot with rough edges. The devices studied are still significantly larger than the presented one.

1 Introduction Graphene nanostructures [1–11] attract increasing attention mainly due to potential applications in high mobility electronics [12, 13] and solid-state quantum information processing [14]. In particular, low nuclear spin concentrations expected in graphene promise long spin lifetimes [14–17] and make graphene quantum dots (QDs) [4–8] interesting for spin-qubit operations [14]. Moreover, graphene nanostructures may allow to investigate phenomena related to massless Dirac Fermions in confined dimensions [5, 18–22]. Intensive research has been triggered by the unique electronic properties of graphene [23] including the gapless linear dispersion, and the unique Landau level (LL) spectrum [24, 25]. The search for signatures of graphene-specific properties in QDs is of interest in order to understand the addition spectra, the spin states and dynamics of confined graphene quasi-particles. Recent advances in fabricating width-modulated graphene nanoribbons helped to overcome intrinsic difficulties in (i) creating tunnelling barriers and (ii) confining electrons in graphene, where transport is dominated by Klein tunnelling-related phenomena [26, 27]. Graphene QDs have been fabricated and Coulomb blockade [4, 5], quantum confinement [7, 8] and charge detection [6] have been observed.

Here, we show tunnelling spectroscopy (i.e. transport) measurements on a fully tunable graphene QD. We present the evolution of a large number of Coulomb resonances near the charge neutrality point in a magnetic field from the low-field regime to the regime of LL formation. In particular, we investigate the QD spectrum in the vicinity of the charge neutrality point as a function of a perpendicular magnetic field (B-field). Near the electron–hole crossover we observe a rich excited state spectrum with inelastic cotunnelling lines and unconventional features inside the Coulomb diamonds. Some of this features, which are very pronounced at $B = 0$, quickly disappear in a perpendicular magnetic field. Moreover, we find indications of the formation of the lowest ($E = 0$) LL at high B-fields marking the electron–hole crossover in graphene devices.

This paper is organized as follows. In Section 2, we briefly review the graphene QD device fabrication. Transport measurements at zero magnetic field are discussed in Section 3.1. LL formation and the magnetic field dependence of inelastic cotunnelling processes are addressed in Sections 3.2 and 3.3, respectively.

2 Device fabrication The state-of-the-art fabrication process of graphene nanodevices, which has been mostly developed in Manchester [24, 28], and in New York [25], is based on the mechanical exfoliation of (natural) graphite by adhesive tapes [28]. The substrate material consists of highly doped silicon (Si^{++}) bulk material covered with approximately 300 nm of silicon oxide (SiO_2), where thickness and roughness of the SiO_2 top layer is crucial for the identification and further processing of single-layer graphene samples. Standard photolithography followed by metalization (chrome/gold) and lift-off is used to pattern arrays of reference alignment markers on the substrate that are later used to re-identify locations (of individual graphene flakes) on the chip and to align further processing patterns.

The graphene flake has to be structured to submicron dimensions in order to fulfil the device design requirements (see, e.g. figure in the abstract). We use a technique based on resist spin coating, electron beam lithography (EBL), development and subsequent etching of the unprotected graphene. Two successive processing steps have been used including small modifications to decrease the minimum feature size of the graphene nanodevice. First we used a resist [polymethylmethacrylate (PMMA)] with a thickness of 45 nm and short etching time to define the delicate structures. In the second step, a 100 nm thick resist is used for the coarse structuring of the flake also providing a broader process parameter window for the etching step. It has been found that short (5 and 15 s) mainly physical reactive ion etching (RIE) based on argon and oxygen (80:20) provides good results without influencing the overall quality of the graphene flake [29]. After etching and removing the residual EBL resist, the graphene nanostructures are contacted by an additional EBL step, followed by metalization and lift-off. Here we evaporated 2 nm chrome (Cr) and 40 nm gold (Au) for contacting the graphene QD device.

A scanning force microscope image of the device studied here is shown as an inset in Fig. 1. The 50 nm wide and 80 nm long graphene QD is connected to source (S) and drain (D) via two graphene constrictions with a width of 25 nm, both acting as tunnelling barriers. The dot and the leads can be further tuned by the highly doped silicon substrate used as a back gate (BG) and an in-plane graphene plunger gate (PG).

3 Measurements All measurements have been performed in a dilution refrigerator at a base temperature of $T \approx 90$ mK. We have measured the two-terminal conductance through the graphene QD device by applying a symmetric DC bias voltage V_b while measuring the current through the QD device with a noise level below 10 fA.

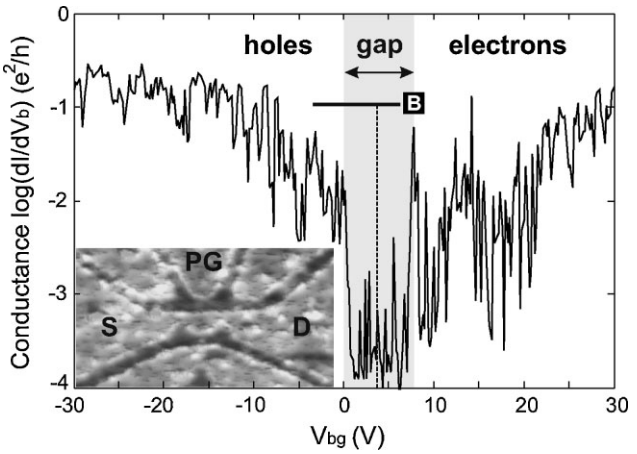

Figure 1 Low bias ($V_b = 100\,\mu$V) BG characteristic at $V_{pg} = 2$ V. The resolved transport gap (see highlighted region) separates between hole and electron transport. This trace is a BG cross-section of fig. 1e in Ref. [8], which includes the region [*B*] marked therein. The dashed line marks the position of the electron–hole crossover identified in Ref. [8]. The inset shows a scanning force microscope image of an etched graphene QD device with source (S) and drain (D) leads and a PG for electrostatic tunability.

For differential conductance measurements, a small AC bias $V_{b,ac} = 40\,\mu$V has been superimposed on V_b and the differential conductance has been measured with lock-in techniques at a frequency of 18.9 Hz.

In Fig. 1, we show the differential conductance as a function of BG voltage at low bias ($V_b = 100\,\mu$V) highlighting the strong suppression of the conductance around the charge neutrality point ($0 < V_{bg} < 7.5$ V) due to the so-called transport gap [30, 31]. Here we tune transport from the deep hole to the deep electron regime, as illustrated in Fig. 1. The large number of resonances within the gap region may be due to both, (i) resonances in the graphene constrictions acting as tunnelling barriers [4] (and thus being main responsible for the large extension of this transport gap) and (ii) Coulomb resonances of the QD itself.

3.1 Coulomb blockade measurements at $B = 0$ By fixing the BG voltage at a value inside the transport gap (e.g. $V_{bg} = -0.9$ V) and sweeping the lateral PG voltage (V_{pg}) in a narrow range close to the charge neutrality point (see below) Coulomb blockade resonances of the graphene QD can be well resolved, as shown in Fig. 2a. The strong amplitude modulation of the conductance peaks (see, e.g. on the very left of Fig. 2a) is mainly due to transparency modulations of the constrictions [4], which can dominate the width of the Coulomb resonances and significantly elevate the conductance. In Fig. 2b, we show corresponding Coulomb diamond measurements (see black bar in Fig. 2a) that are measurements of the differential conductance ($G_{qd} = dI/dV_b$) as a function of bias voltage V_b and PG voltage V_{pg}. Note that this measurement was recorded at a higher base temperature of $T = 370$ mK. The reason for this slightly higher temperature is the good

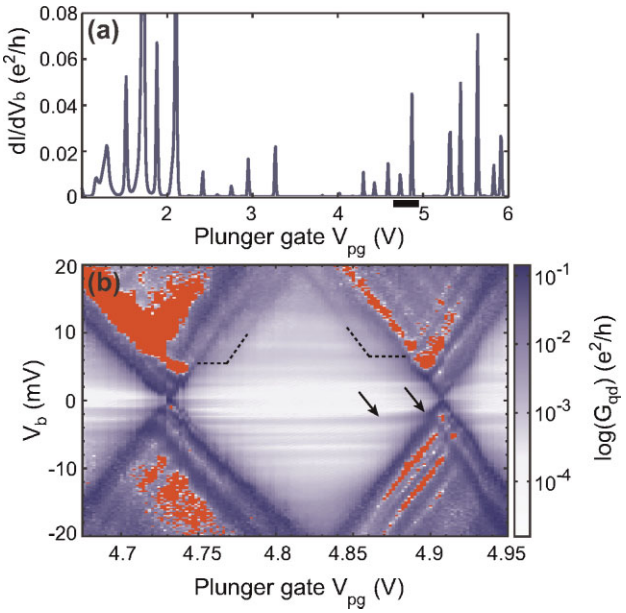

Figure 2 (online colour at: www.pss-b.com) (a) Coulomb blockade resonances of the graphene QD as function of PG voltage V_{pg} at $V_{bg} = -0.9$ V. The conductance has been measured at constant bias of $V_b = 100\,\mu$V. (b) Coulomb diamonds, i.e. finite-bias measurement of the QDs differential conductance $G_{qd} = dI/dV_b$ as function of V_b and V_{pg} at $B = 0$. Note the rich excited state spectra and in particular the different vertical distances between the diamond edge and the diagonal structures inside the Coulomb-blockaded region for positive V_b.

visibility of the diagonal lines inside the diamond. The overall structure of the diamond is not changed significantly by increasing the temperature. The logarithmic plot of the Coulomb diamonds measured in the close vicinity of the charge neutrality point displays a rich excited states spectrum. We observe lines of increased conductance outside the diamonds running parallel to the diamond edges, which are well aligned to inelastic cotunnelling onsets visible as faint horizontal (constant bias) structures inside the diamond-shaped regions (see arrows). At the diamond boundary, the horizontal lines seamlessly join some of the most prominent diagonal lines in the nonblockaded region, allowing to extract characteristic excitation energies in the range of 2–3 meV.

In addition, we observe for positive bias $V_b > 0$ V unconventional features inside the Coulomb-blockaded regions (see dashed lines) consisting of diagonal lines running parallel to the diamond edge. The fact that they have the same slope as the diamond edges suggests that they are connected to the alignment of an energy level with source (negative slope) or drain (positive slope). The vertical distance between the diagonal lines and the diamond edge is identical for lines with positive (see dashed line inside the diamond) and negative slope. It has been shown by Schleser et al. [32] that these features are related to sequential tunnelling through the QD, occurring after it has been excited by an inelastic cotunnelling process. In simple terms, these features can be attributed to a transport configuration where the tunnelling-out rate from the excited state is significantly larger than the relaxation rate to the ground state, which might be directly related to strongly nonlinear energy dependences of the tunnelling barriers. Finally, we also observe regions of negative differential conductance, which are not yet fully understood.

3.2 Coulomb resonances as a function of a perpendicular magnetic field In Fig. 3, we show more than 40 Coulomb resonances as a function of a B-field perpendicular to the graphene plane. The measurement has been taken in the BG voltage range from $V_{bg} = -3.5$ to 6 V (also highlighted by the vertical line [B] in Fig. 1 and fig. 1e in Ref. [8]). Thus we certainly tune from hole to electron transport (see arrows in Fig. 1). The evolution of Coulomb resonances in (perpendicular) magnetic field shows signatures of the electron–hole crossover of the QD states (see below and Ref. [8]). There is a common trend of resonances at lower BG voltages (see, e.g. resonances at $V_{bg} = 0$ V) to bend for increasing B-field towards higher energies (higher V_{bg}). In contrast we find for higher BG voltage the opposite trend (see, e.g. resonances and arrow at $V_{bg} \approx 5.8$ V), where resonances tend to shift to lower energies for increasing magnetic field. This overall pattern is disturbed by additional features such as localized states, regions of multi-dot behaviour and strong amplitude modulations due to constriction resonances. For example, we observe a strongly elevated background below $V_{bg} < -1$ V, which can be attributed to the increase of the transparency of the tunnelling barriers in agreement with the measurement presented in

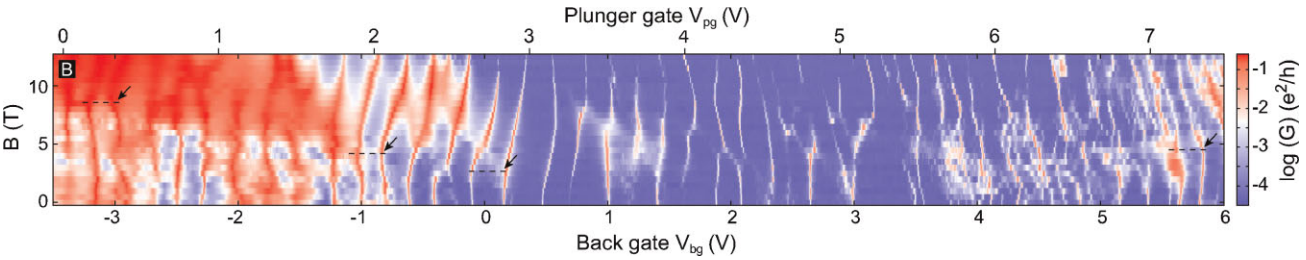

Figure 3 (online colour at: www.pss-b.com) Evolution of Coulomb blockade resonances in perpendicular magnetic field. The conductance is plotted as function of BG voltage V_{bg} and magnetic field B ($V_b = 500\,\mu$V). The effective PG voltage V_{pg}, calculated via the relative lever arm, is given on the top of the graph. This data have been measured in the regime marked by the solid line [B] in Fig. 1e of Ref. [8].

Fig. 1. Additionally, we observe between $V_{bg} = -1$ and 0 V a weakly coupled state crossing the Coulomb resonances at finite magnetic fields. We interpret the weak magnetic field dependence and low visibility in transport as a manifestation of a strongly localized state. Moreover, we see several level crossings and splittings in the region above $V_{bg} = 4$ V, which might be due to the presence of an additional QD spontaneously forming in one of the two constrictions, and coupling to the gates with different lever arms [8].

Finally, in close analogy to Ref. [8] where the same sample was investigated in a different parameter regime we observe 'kink' features with increasing B-field. It has been found that with increasing magnetic field the levels feature a kink signifying filling factor $\nu = 2$ in the dot (see dashed lines and arrows in Fig. 3) before converging toward the $E = 0$ LL, in analogy to what has been observed in GaAs QDs [33]. In particular, the population of the lowest LL leads to a region around $E = 0$ [8, 34] with a remarkably ordered addition spectrum, which emerges for large magnetic fields (see also the analytical calculations for a circular dot [19, 20]). This feature is a unique consequence of the interplay of the unique LL spectrum in graphene [24, 25] and the carrier confinement due to the finite size of the system. For more details, including numerical simulations of graphene QDs and a quantitative discussion of the peak-to-peak spacing evolution in B-field we refer to Refs. [8, 34].

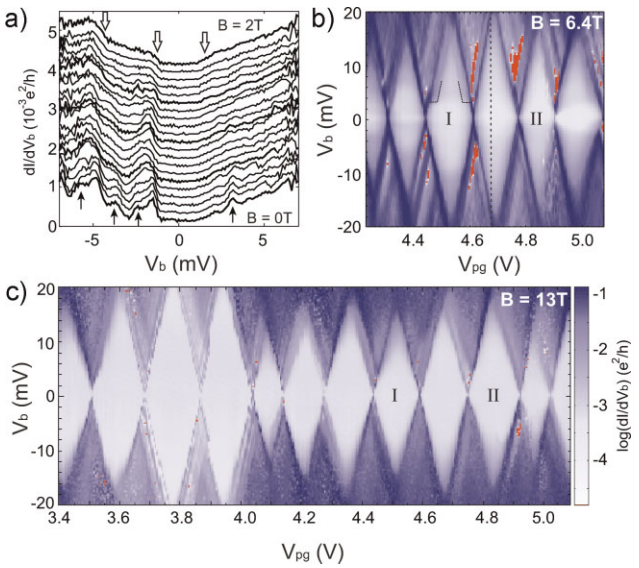

Figure 4 (online colour at: www.pss-b.com) (a) Evolution of inelastic cotunnelling onsets inside the Coulomb-blockaded region in perpendicular magnetic field. The conductance is plotted as function of bias V_b and magnetic field $B = 0$ to 2 T (stepped in units of 0.1 T) for constant PG voltage $V_{pg} = 4.66$ V [see vertical line in panel (b)]. For clarity the individual traces have been offset by 0.2×10^{-3} e^2/h. The peaks related to inelastic cotunnelling marked by arrows quickly vanish as function of B. (b,c) Coulomb diamond measurements at $B = 6.4$ T (b) and $B = 13$ T (c), respectively. These measurements are taken at constant BG voltage $V_{bg} = -0.9$ V and highlight both (i) single dot signatures at high magnetic fields and (ii) the strong suppression of excited state-related signatures at higher B-fields.

3.3 Coulomb diamonds at finite magnetic field In Fig. 4a, we show the evolution of inelastic cotunnelling onsets inside the Coulomb-blockaded region as a function of perpendicular magnetic field. The conductance is plotted as a function of bias voltage V_b and magnetic field at constant PG voltage $V_{pg} = 4.66$ V (see vertical line in Fig. 4b) and the B-field has been stepped by 0.1 T from $B = 0$ to 2 T. While at $B = 0$ T we observe several steps and peaks (black and white arrows), at $B = 2$ T the trace is smoother with remaining steps at 1.4, −1.3 and 4.5 mV (white arrows). The different B-field dependence of the features might be attributed to two origins. The fine structures disappearing at $B = 0.15$ T (black arrows) may arise from energy dependent fluctuations of the barrier transmission, while the steps (white arrows) are attributed to the onset of inelastic cotunnelling channels. This is supported by Figs. 4b,c, where we show Coulomb diamond measurements at $B = 6.4$ and 13 T. These measurements are taken at the same constant BG voltage $V_{bg} = -0.9$ V as in Fig. 2b and are plotted with the same colourscale. Thus, we can directly compare Figs. 2b, 4b and 4c simplified by the diamond labels I and II (see Figs. 4b,c; the diamond shown in Fig. 2b corresponds to diamond II). The horizontal (constant bias) lines in the Coulomb blockaded region present at $B = 0$ T are absent at higher B-fields. However, at $B = 6.4$ T cotunnelling onsets and the unconventional feature consisting of diagonal lines inside the diamond (see above and dashed lines in Fig. 4b) can still be observed, but in a different diamond than at $B = 0$ T (I instead of II). At $B = 13$ T all excited-state related signatures inside the diamond are suppressed. In addition, also the negative differential conductance outside the diamond is significantly reduced and might too be related to a decrease in the energy dependent fluctuation of the barrier transmission. However, from these measurements we can conclude that the single-dot behaviour of the etched graphene QD device stays well preserved also for high magnetic fields.

4 Conclusion We have performed detailed studies of transport through a graphene QD in the vicinity of the charge neutrality point. The evolution of Coulomb resonances in magnetic field showed signatures of LL formation. Indications for the crossing of filling factor $\nu = 2$ are obtained by the observation of 'kinks' in spectral lines before bending towards the charge neutrality point. Coulomb blockade diamonds at $B = 0$ T near the electron–hole crossover show many excited states and cotunnelling onsets accompanied by diagonal lines in the diamond attributed to cotunnelling mediated sequential tunnelling through an excited state. Many small scale lines inside the diamond disappear quickly ($B = 1.5$ T) in a magnetic field while more step like features (cotunnelling onsets) are still visible at $B = 6.4$ T. The presented measurements open the way for an in-depth

exploration of the few charge carrier regime including addition spectra in graphene QDs.

Acknowledgements The authors wish to thank F. Libisch, J. Seif, P. Studerus, C. Barengo, T. Helbling and S. Schnez for help and discussions. Support by the ETH FIRST Lab, the Swiss National Science Foundation and NCCR nanoscience are gratefully acknowledged.

References

[1] M. Y. Han, B. Özyilmaz, Y. Zhang, and P. Kim, Phys. Rev. Lett. **98**, 206805 (2007).
[2] Z. Chen, Y.-M. Lin, M. Rooks, and P. Avouris, Physica E **40**, 228 (2007).
[3] X. Li, X. Wang, L. Zhang, S. Lee, and H. Dai, Science **319**, 1229 (2008).
[4] (a) C. Stampfer, J. Güttinger, F. Molitor, D. Graf, T. Ihn, and K. Ensslin, Appl. Phys. Lett. **92**, 012102 (2008).
(b) C. Stampfer, E. Schurtenberger, F. Molitor, J. Güttinger, T. Ihn, and K. Ensslin, Nano Lett. **8**, 2378 (2008).
[5] L. A. Ponomarenko, F. Schedin, M. I. Katsnelson, R. Yang, E. H. Hill, K. S. Novoselov, and A. K. Geim, Science **320**, 356 (2008).
[6] J. Güttinger, C. Stampfer, S. Hellmüller, F. Molitor, T. Ihn, and K. Ensslin, Appl. Phys. Lett. **93**, 212102 (2008).
[7] S. Schnez, F. Molitor, C. Stampfer, J. Güttinger, I. Shorubalko, T. Ihn, and K. Ensslin, Appl. Phys. Lett. **94**, 012107 (2009).
[8] J. Güttinger, C. Stampfer, F. Libisch, T. Frey, J. Burgdörfer, T. Ihn, and K. Ensslin, Phys. Rev. Lett. **103**, 046810 (2009).
[9] K. Todd, H.-T. Chou, S. Amasha, and D. Goldhaber-Gordon, Nano Lett. **9**, 416 (2009).
[10] X. Liu, J. Oostinga, A. F. Morpurgo, and L. M. K. Vandersypen, Phys. Rev. B **80**, 121407(R) (2009).
[11] K. A. Ritter and J. W. Lyding, Nature Mater. **8**, 235 (2009).
[12] A. K. Geim and K. S. Novoselov, Nature Mater. **6**, 183 (2007).
[13] M. I. Katnelson, Mater. Today **10**(1–2), 20 (2007).
[14] B. Trauzettel, D. V. Bulaev, D. Loss, and G. Burkard, Nature Phys. **3**, 192 (2007).
[15] C. L. Kane and E. J. Mele, Phys. Rev. Lett. **95**, 226801 (2005).
[16] H. Min, J. E. Hill, N. A. Sinitsyn, B. R. Sahu, L. Kleinman, and A. H. MacDonald, Phys. Rev. B **74**, 165310 (2006).
[17] D. Huertas-Hernando, F. Guinea, and A. Brataas, Phys. Rev. B **74**, 155426 (2006).
[18] M. V. Berry and R. J. Mondragon, Proc. R. Soc. Lond. A **412**, 53 (1987).
[19] S. Schnez, K. Ensslin, M. Sigrist, and T. Ihn, Phys. Rev. B **78**, 195427 (2008).
[20] P. Recher, J. Nilsson, G. Burkard, and B. Trauzettel, Phys. Rev. B **79**, 085407 (2009).
[21] F. Libisch, C. Stampfer, and J. Burgdörfer, Phys. Rev. B **79**, 115423 (2009).
[22] A. F. Young and P. Kim, Nature Phys. **5**, 222 (2009).
[23] For review see, A. H. Castro Neto, F. Guinea, N. M. Peres, A. K. Geim, Rev. Mod. Phys. **81**, 109 (2009).
[24] K. S. Novoselov, A. K. Geim, S. V. Morozov, D. Jiang, M. I. Katsnelson, I. V. Grigorieva, S. V. Dubonos, and A. A. Firsov, Nature **438**, 197 (2005).
[25] Y. Zhang, Y.-W. Tan, H. L. Stormer, and P. Kim, Nature **438**, 201 (2005).
[26] N. Dombay and A. Calogeracos, Phys. Rep. **315**, 41 (1999).
[27] M. I. Katsnelson, K. S. Novoselov, and A. K. Geim, Nature Phys. **2**, 620 (2006).
[28] K. S. Novoselov, A. K. Geim, S. V. Morozov, D. Jiang, M. I. Katsnelson, S. V. Dubonos, I. V. Grigorieva, and A. A. Firsov, Science **306**, 666 (2004).
[29] F. Molitor, J. Güttinger, C. Stampfer, D. Graf, T. Ihn, and K. Ensslin, Phys. Rev. B **76**, 245426 (2007).
[30] C. Stampfer, J. Güttinger, S. Hellmüller, F. Molitor, K. Ensslin, and T. Ihn, Phys. Rev. Lett. **102**, 056403 (2009).
[31] F. Molitor, A. Jacobsen, C. Stampfer, J. Güttinger, T. Ihn, and K. Ensslin, Phys. Rev. B **79**, 075426 (2009).
[32] R. Schleser, T. Ihn, E. Ruh, K. Ensslin, M. Tews, D. Pfannkuche, D. C. Driscoll, and A. C. Gossard, Phys. Rev. Lett. **94**, 206805 (2005).
[33] M. Ciorga, A. S. Sachrajda, P. Hawrylak, C. Gould, P. Zawadzki, S. Jullian, Y. Feng, and Z. Wasilewski, Phys. Rev. B **61**, R16315 (2000).
[34] F. Libisch, S. Rotter, J. Güttinger, C. Stampfer, K. Ensslin, and J. Burgdörfer, in preparation.